A theoretical investigation of the increase in venous oxygen saturation levels in advanced glaucoma patients

Lucia Carichino[1], Alon Harris[2], Giovanna Guidoboni[1,2,3], Brent A. Siesky[2], Luis Abegão Pinto[7], Evelien Vandewalle[5], Olof B. Olafsdottir[4], Sveinn H. Hardarson[4], Karel Van Keer[5], Ingeborg Stalmans[5,6], Einar Stefánsson[4], Julia C. Arciero[1]

[1]Department of Mathematical Sciences, Indiana University - Purdue University Indianapolis, Indianapolis, IN, USA; [2]Department of Ophthalmology, Indiana University School of Medicine, Indianapolis, IN, USA; [3]LABEX Institut de Recherche en Mathématiques, Interactions et Applications, Strasbourg, France; [4]Department of Ophthalmology, University of Iceland, Reykjavik, Iceland; [5]Department of Ophthalmology, University Hospitals Leuven, Leuven, Belgium; [6]Department of Ophthalmology Neurosciences, Laboratory of Ophthalmology, Katholieke Universiteit Leuven, Leuven, Belgium; [7]Department of Ophthalmology, Centro Hospitalar Lisboa Norte, Lisbon, Portugal

Abstract

Purpose: Vascular changes have been observed among glaucoma patients, but it is not yet known whether these vascular changes occur primary or secondary to glaucomatous damage. In this study, a theoretical mathematical model of the retinal vasculature is applied to a set of oximetry data obtained from healthy individuals and glaucoma patients and is used to propose possible explanations for the clinically observed increases in venous blood oxygen saturation in advanced glaucoma patients.
Methods: Given clinical measurements of intraocular pressure (IOP), mean arterial pressure and arterial blood oxygen saturation from healthy persons and advanced (visual field mean defect (MD) ≥ 10 dB) primary open angle glaucoma (POAG, IOP > 21 mmHg) patients and advanced normal tension glaucoma (NTG, IOP ≤ 21 mmHg)

Correspondence: Julia C. Arciero, Department of Mathematical Sciences, 402 N. Blackford St., LD 270 D Indianapolis, IN 46202-3267, USA.
E-mail:jarciero@math.iupui.edu.

patients, the model is used to predict the oxygen demand or Krogh cylinder tissue width that would yield the clinically-measured venous oxygen saturation in each population.

Results: A decrease in retinal tissue oxygen demand (M_0), an impairment in blood flow autoregulation, or a decrease in Krogh cylinder tissue width (d) can independently lead to increased venous saturation. The model predicts that a decrease in M_0 or a decrease in d is more likely to yield the increased venous saturation levels observed in POAG patients, while impairing blood flow autoregulation with no change in M_0 or d is more likely to yield the increased venous saturation levels observed in NTG patients.

Conclusions: The combined theoretical and clinical model predictions suggest that the mechanisms leading to increased venous saturation might differ between POAG and NTG patients. The model predictions are used to hypothesize that a decrease in oxygen demand might be more relevant to the increase in venous saturation observed in advanced POAG, while impairment in autoregulation mechanisms might be more relevant to the increase in venous saturation observed in advanced NTG.

Keywords: blood flow autoregulation, glaucoma, mathematical model, oximetry, oxygen saturation, oxygen consumption, retina, spectrophotometry

1. Introduction

Glaucoma is a progressive optic neuropathy associated with visual field loss and retinal ganglion cell death. Although glaucoma progression has been primarily associated with elevated levels of intraocular pressure (IOP), recent studies have suggested that metabolic alterations, dysfunctions of vascular autoregulation and changes in oxygen supply to tissue are also relevant factors to be considered in the progression of the disease.[1,2] The correlations between retinal metabolic alterations and vision loss are not yet fully understood; however, alterations in the retinal blood oxygen saturation levels of glaucomatous patients have been observed.[3-6] Also, blood flow deficiencies reported in retinal and retrobulbar vessels[7-11] of glaucoma patients support the hypothesis that hemodynamic alterations are correlated to glaucoma damage, independent of or related to IOP.[12,13] Alterations in the micro-vascular network density (and thus oxygen supply to tissue) in the optic disc and temporal areas have also been reported in glaucoma patients when compared with healthy individuals.[14-16]

Despite this evidence linking blood flow alterations with glaucoma, it is still unknown whether vascular changes occur primary or secondary to retinal ganglion cell loss. If primary, impaired autoregulation or insufficient blood supply to the retina and optic nerve would lead to tissue damage with subsequent vision loss. If secondary, vascular changes would be the result of optic nerve damage and the

loss of retinal ganglion cells, since those cells would no longer require oxygen or nutrient.

Several techniques can be used to measure vascular alterations in the eye, including fluorescein angiography, color Doppler imaging, laser Doppler flowmetry, Doppler optical coherence tomography and retinal oximetry.[2,17,18] In particular, retinal oximetry can be used to measure hemoglobin oxygen saturation and vessel diameters in the retina.[4,6,19-22] While many oximetry studies[4,6,19-22] have been conducted among healthy individuals and patients with various types and severity of glaucoma, trends in the oximetry measurements were not consistent across studies. For example, some studies[6,19] found no differences in venous oxygen saturation levels of normal-tension glaucoma (NTG) and high-tension primary open-angle glaucoma (POAG) patients when compared with the levels in healthy individuals, while other studies[4,20-22] found significant differences in venous oxygen saturation among these populations.

In three studies,[3,4,20] patients with advanced glaucoma (visual field mean defect (MD) ≥ 10 dB) exhibited higher venous oxygen saturation levels (and thus a lower arteriovenous difference in oxygen saturation) compared with healthy individuals and mild glaucoma patients (MD ≤ 5 dB). These observations led to the hypothesis that the decreased arteriovenous difference in the advanced glaucoma group could be due to a decrease in retinal oxygen consumption, but additional and preferably longitudinal studies in glaucoma patients are necessary to help to distinguish if the observed vascular changes occur primary or secondary to glaucoma damage.

As evident from the inconsistent trends in reported clinical data, additional methods are needed before definitive conclusions can be made relating blood oxygen saturation changes and the severity or type of glaucoma. This study applies a previously developed theoretical model of retinal vascular wall mechanics[23] to a set of clinical oximetry data obtained from healthy individuals and glaucoma patients[4] to propose possible explanations for the increases in venous oxygen saturation observed in advanced glaucoma patients. The combined mathematical and clinical approach is used to calculate theoretical changes in blood oxygen saturation in retinal arterioles, capillaries and venules and to compute patient-specific levels of tissue oxygen demand or Krogh tissue width (herein referred to as "tissue width") that would yield the measured values of venous oxygen saturation given values of mean arterial pressure (MAP = (2*DBP+SBP)/3, where DBP is diastolic blood pressure and SBP is systolic blood pressure), IOP and arterial oxygen saturation from patients. The resulting theoretical predictions provide a wider range of possible factors that could explain clinical observations than would be intuitive, and these results offer an important step in distinguishing between the primary causes and secondary effects of glaucoma.

2. Methods

2.1 Experimental data

Retinal oximetry is a clinical technique used to assess oxygen saturation levels and vessel caliber in individuals with various ocular diseases. This study focuses on oximetry data in patients with different types and degrees of severity of glaucoma. The methods of performing retinal oximetry and obtaining baseline measurements of factors such as IOP and blood pressure in glaucoma patients and healthy individuals has previously been described in detail.[4] In short, measurements from 89 healthy individuals and 74 glaucoma patients of age 40 years or older were collected. Individuals with systemic diseases or ocular diseases other than open angle glaucoma were excluded from the study. However, patients receiving antihypertensive medication for elevated systemic blood pressure and patients with mild cataracts were not excluded.

Glaucoma was defined based on the characteristic optic disc damage and the corresponding visual field defects. Of all of the glaucoma patients considered in this study, 45 were diagnosed with POAG and 29 were diagnosed with NTG. A diagnosis of POAG was defined by an untreated IOP > 21 mmHg. Patients with IOP measurements consistently ≤ 21 mmHg were classified as having NTG. All glaucoma patients underwent automated perimetry. A patient was defined as having "mild glaucoma" if the visual field mean defect (MD) was ≤ 5 dB and was defined as having "advanced glaucoma" if the visual field MD ≥ 10 dB. Of the 45 POAG patients, 20 were diagnosed with mild glaucoma and 12 were diagnosed with advanced glaucoma. Of the 29 NTG patients, 13 were diagnosed with mild glaucoma and 9 were diagnosed with advanced glaucoma. Some patients were under active treatment at the time of measurement.

All oximetry measurements were performed in darkness with the Oxymap T1 oximeter (Oxymapehf, Reykjavik, Iceland), where relative oxygen saturation was measured semi-automatically with the Oxymap Analyzer Software 2.2.1 (v.3847). The IOP measurements were performed on dilated pupils using a Goldmann applanation tonometry mounted on a Haag-Streit slit lamp (Haag-Streit BQ 900, Haag-Streit International, Köniz, Switzerland) in Belgium, and using the iCare TAO1 tonometer (Tiolat Oy, Helsinki, Finland) in Iceland. An automatic sphygmomanometer was used to obtain all measurements of systolic and diastolic blood pressures after a 5 min resting period (in Belgium: Omron HEM-7001-E, Omron, Kyoto, Japan; in Iceland: Omron HEM-7221-E, Omron, Kyoto, Japan).

2.2 Mathematical model

To determine possible explanations for measured changes in venous oxygen saturation in POAG and NTG patients,[4] a simplified mathematical model of the retinal vasculature, previously developed by Arciero et al.,[23] is used. The retinal vasculature downstream of the central retinal artery (CRA) and upstream of the central retinal
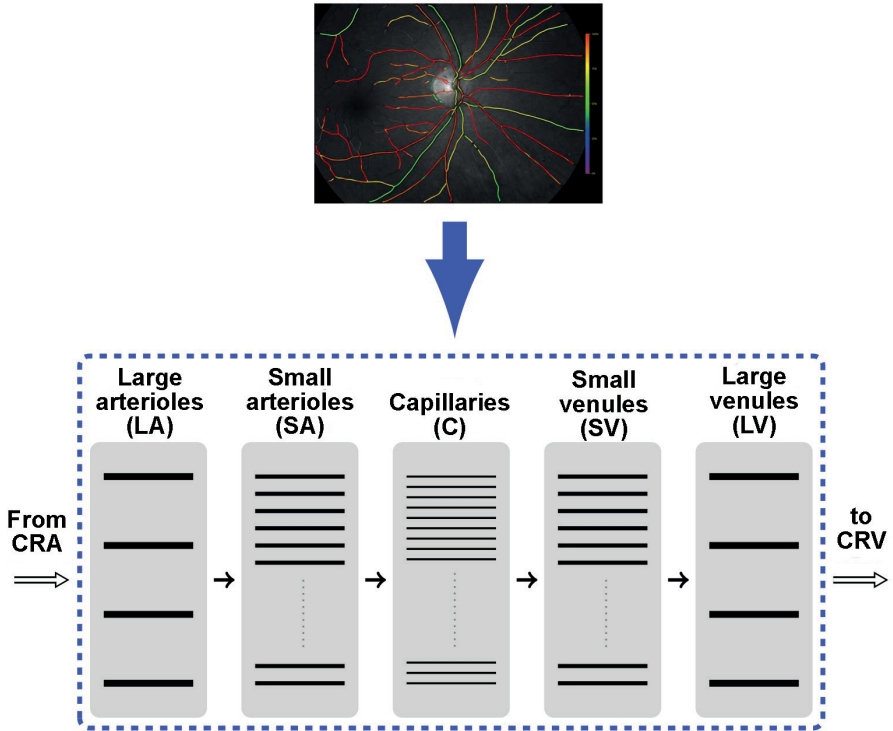
Fig. 1. The retinal vasculature, as depicted in the oximetry image (top), is modeled as a representative segment network (bottom) consisting of five compartments of parallel-arranged vessels connected in series downstream of the central retinal artery (CRA) and upstream of the central retinal vein (CRV): Large arterioles/arteries (LA), small arterioles (SA), capillaries (C), small venules (SV) and large venules/veins (LV).

vein (CRV) is modeled as a representative segment network, where five vessel compartments for the large arterioles (LA), small arterioles (SA), capillaries (C), small venules (SV) and large venules (LV) supplying and draining the retina are connected in series; each compartment consists of identical segments arranged in parallel (Fig. 1). All compartments are assumed to experience the same hemodynamic and metabolic conditions. A summary of the model equations, along with its input values and output values, is provided in Table 1. The subscripts used in Table 1 indicate if the quantity is evaluated either at the inlet (*in,i*), midpoint (*mp,i*) or outlet (*out,i*) of the *i*th compartment, where *i*=LA,SA,C,SV,LV. The values of the model parameters are listed in Tables 2, 3 and 4. In the following, the main features of the model are discussed, which are leveraged to perform the simulations reported in the Results section. For a complete description of the model we refer to a previous study by Arciero *et al.*[23]

Table 1. Summary of model[23] variables and equations (sections b – f), including input (section a) and output (section g) data.

	Input
(a)	$P_{in,LA} = \frac{2}{3}MAP - 20\text{mmHg}, \quad P_{out,LV} = IOP, \quad S(x=0) = \text{arterial oxygen saturation},$
	$M_0, \quad d, \quad bCO_2(x=0) = 50\%, \quad C(x=0) = 0.5\mu M$

		Equations
(b)		$\begin{cases} \dfrac{dD_i}{dt} = \dfrac{2\lambda_i}{\tau_d}\left(T_i - T_{total,i}\right) \\ \dfrac{dA_i}{dt} = \dfrac{1}{\tau_a}\left(A_{total,i} - A_i\right) \end{cases} \quad i = \text{LA,SA}$

$T_{total,i} = T_{passive,i} + A_i T_{max.active,i} \qquad\qquad T_{passive,i} = C_{pass,i}\exp\left[C'_{pass,i}\left(D_i/D_{0,i} - 1\right)\right]$

$T_{max.active,i} = C_{act,i}\exp\left\{-\left[\left(D_i/D_{0,i} - C'_{act,i}\right)/C''_{act,i}\right]^2\right\} \qquad A_{total,i} = 1/\left(1 + \exp(-S_{tone,i})\right)$

$$S_{tone,i} = C_{myo,i}T_i - C_{shear,i}\tau_i - C_{meta,i}S_{CR,i} - C_{CO_2,i}S_{CO_2,LV} + C''_{tone,i}$$

(c)	Myogenic	$T_i = (P_{mp,i} - IOP)D_i/2 \quad i = \text{LA,SA,C,SV,LV}$
		$\Delta P_{tot} = Q_{tot}R_{tot} = P_{in,LA} - P_{out,LV} \quad R_{tot} = \sum_i R_i \quad Q_{tot} = n_i Q_i$
		$\Delta P_i = Q_i R_i = P_{in,i} - P_{out,i} \quad R_i = (128\mu_i L_i)/(\pi D_i^4 n_i) \quad P_{mp,i} = P_{in,i} + \frac{1}{2}\Delta P_i$

(d)	Shear stress	$\tau_i = (32\mu_i Q_i)/(\pi D_i^3) \quad i = \text{LA,SA,C,SV,LV}$

(e)	Metabolic	$S_{CR,i} = \displaystyle\int_{x_{mp,i}}^{x_{end,i}} \exp\left[-(y - x_{mp,i})/L_0\right]C(y)dy \quad i = \text{LA,SA}$

$C(x) = \alpha + \beta(x - x_{in,i}) + \exp\left[\gamma(x_{in,i} - x)\right](C(x_{in,i}) - \alpha)$

$\alpha(x) = H_T R_0\left[D_i(1 - R_1 S(x_{in,i})) - (1 - H_D)R_0 q(x)/(\pi c_0 H_D k_d)\right]/4k_d$

$\beta(x) = (D_i H_T R_0 R_1 q(x))/(4Q_i c_0 H_D k_d) \qquad \gamma = k_d \pi D_i/[(1 - H_D)Q_i]$

$q(x) = M_0\pi(r_{t,i}^2 - r_{v,i}^2) \qquad r_{v,i} = \frac{1}{2}D_i \qquad r_{t,i} = r_{v,i} + d_i$

$S(x) = S(x_{in,i}) + q(x)(x_{in,i} - x)/(Q_i c_0 H_D)$

$PO_2(x,r) = PO_2(x, r_{v,i}) + M_0\left[(r^2 - r_{v,i}^2)/4 + r_{t,i}^2\ln(r_{v,i}/r)/2\right]/k$

(f)	Carbon dioxide	$S_{CO_2,LV} = f(PCO_{2LV}, Q_{tot})$
		$PCO_{2LV} = g(tCO_2(x_{mp,LV})) \qquad tCO_2(x) = bCO_2(x)(1 - (-0.115Q_{tot} + 0.23))$
		$bCO_2(x) = bCO_2(x_{in,i}) - 0.81q(x)(x_{in,i} - x)/(Q_i c_0 H_D)$

	Output
(g)	$P_i, \Delta P_i, R_i \text{ and } Q_i \ i = \text{LA,SA,C,SV,LV}, \ C(x), \ S(x), \ PO_2(r,x), \ tCO_2(x), \ bCO_2(x)$

Table 2. Parameter values for passive tension, active tension, and vascular smooth muscle activation equations in the large arterioles (LA) and small arterioles (SA).

Constant	Value		Unit	Constant	Value		Unit
	LA	SA			LA	SA	
C_{pass}	361.48	197.01	$[dyn/cm]$	C_{myo}	0.0092	0.025	$[cm/dyn]$
C'_{pass}	53.69	17.60	$[1]$	C_{shear}	0.0258	0.0258	$[cm^2/dyn]$
C_{act}	2114.2	3089.6	$[dyn/cm]$	C_{meta}	200	200	$[\mu M/cm]$
C'_{act}	0.93	1.02	$[1]$	C_{co_2}	8e^{-4}	1.31e^{-4}	$[1/mmHg]$
C''_{act}	0.11	0.20	$[1]$	C''_{tone}	159.26	62.27	$[1]$
λ	0.0457	0.0604	$[1/mmHg]$	D_0	135.59	73.9	$[\mu M]$

Table 3. Time constants for the model equations (Table 1(b)) and parameter values for the metabolic response (Table 1(e)).

Parameter	Value	Unit
time constant for diameter, τ_d	1	$[s]$
time constant for activation, τ_a	60	$[s]$
tube hematocrit, H_T	0.3	$[1]$
discharge hematocrit, H_D	0.4	$[1]$
rate of ATP degradation, k_d	2e^{-4}	$[cm/s]$
maximum rate of ATP release, R_o	1.4e^{-9}	$[mol\ s^{-1}\ cm^{-3}]$
effect of oxygen saturation on ATP release, R_1	0.891	$[1]$
oxygen capacity of red blood cells, c_0	0.5	$[cm^3\ O_2/cm^3]$
oxygen tissue diffusion coefficient, k	9.4	$[cm^3\ O_2\ cm^{-1}\ mmHg^{-1}\ s^{-1}]$
length constant for S_{cr}, L_0	1	$[cm]$

Table 4. Parameter values describing vessel network geometry and viscosity.

Parameter	Value					Unit
	LA	SA	C	SV	LV	
number of segments, n	4	39	111,360	39	4	$[1]$
segment length, L	0.807	0.583	0.088	0.583	0.807	$[cm]$
viscosity, μ	2.28	2.06	10.01	2.09	2.44	$[cP]$

Blood flow and oxygen saturation throughout the network are predicted according to hemodynamic and mechanical principles. Retinal flow is assumed to follow Poiseuille's Law, in which flow through each vessel is proportional to the fourth power of the vessel diameter. The complex blood rheology is accounted for by assigning different values of the apparent viscosity μ to vessels in each compartment according to an experimental *in vivo* relationship[24] (Table 4). The total tension $T_{total,i}$ generated in the vessel walls of the vasoactive compartments i= LA, SA follows the Law of Laplace and is modeled as the sum of passive and active tension, denoted by $T_{passive,i}$ and $T_{max.active,i}$, respectively, as detailed in Table 1(b). $T_{passive,i}$ results from the structural components of the vessel wall, and $T_{max.active,i}$ is generated by the contraction and dilation of smooth muscles in the LA and SA. Smooth muscle tone in LA and SA is described by the activation function $A_{total,i}$, which ranges from 0 to 1. The product of $T_{max.active,i}$ and the activation A_i yields the active tension generated in the vessel wall. Changes in $A_{total,i}$ are dictated by the stimulus function $S_{tone,i}$ which results from a linear combination of four autoregulatory mechanisms:

1. *myogenic mechanism*, related to the wall tension T_i computed via the Law of Laplace. Details are provided in Table 1(c), where ΔP_{tot} represents the total pressure drop along the retinal network from the outlet of the CRA to the inlet of the CRV, and ΔP_i represents the pressure drop along each segment of the ith compartment. Similarly, Q_{tot} represents the total blood flow along the network and Q_i represents the blood flow in each segment of the ith compartment, and R_{tot} represents the resistance to flow offered by the whole retinal network and R_i represents the resistance to flow offered by a single segment of the ith compartment. The resistances R_i are computed according to Poiseuille's Law;
2. *shear stress mechanism*, related to the wall shear stress τ_i computed according to Poiseuille's Law. Details are provided in Table 1(d);
3. *metabolic mechanisms*, related to the signal $S_{CR,i}$. Details are provided in Table 1(e), where the signal $S_{CR,i}$ depends on the ATP concentration at each position x along the network $C(x)$, which itself depends on the blood oxygen saturation at each point in the network $S(x)$;
4. *carbon dioxide mechanism*, related to the signal $S_{CO_2,LV}$. Details are provided in Table 1(f), where the signal $S_{CO_2,LV}$ is given by the nonlinear function f of the partial pressure of carbon dioxide in the tissue (PCO_2) and of the total retinal blood flow (Q_{tot}). The tissue carbon dioxide content (tCO_2) is converted into PCO_2 via carbon dioxide dissociation curves, represented by the function g. The tissue carbon dioxide content and the blood carbon dioxide content (bCO_2) are assumed to be linearly related.[25]

The vasodilatory effect of nitric oxygen and the vasoconstrictor effect of endothelin-1 released by endothelial cells[1] is not modeled explicitly. The roles of

these endothelial drivers for autoregulation has been established in the anterior optic nerve region,[26,27] but less is known about their roles in the retinal microcirculation and thus these factors are neglected here.

Arciero *et al.*[23] showed that the metabolic and carbon dioxide responses contribute most significantly to blood flow autoregulation, leading to a nearly constant blood flow over a wide range of intraluminal pressures. In the model, autoregulation is achieved through changes in the diameters D_i of the LA and SA segments, which should be interpreted as the new equilibrium state attained by the system as the input data are altered. In this study, simulations are also performed in the case of impaired autoregulation corresponding to the case in which metabolic and carbon dioxide mechanisms are switched off.

Since the present study aims to compare model-predicted and clinically measured venous saturation levels, details for the oxygen saturation model calculations are provided. Other details of flow, diameter and smooth muscle activation calculations are given previously[23] and are outlined here in Table 1.

By the conservation of mass, the change in oxygen flux must equal the rate of oxygen consumed by the retinal tissue:

$$\frac{d}{dx}[Q_i c_0 H_D S(x)] = -q(x) \tag{1}$$

where x is the distance along the network, Q_i is the blood flow in each compartment
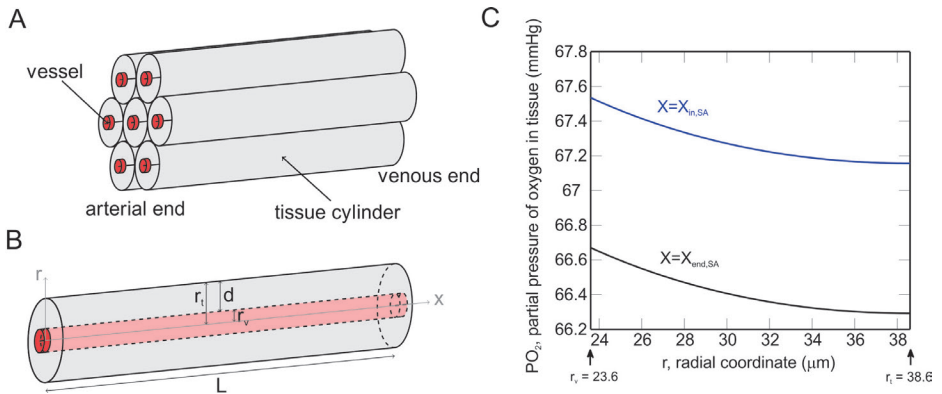
Fig. 2. A Krogh cylinder model is used to predict oxygen diffusion in retinal tissue. A) Representation of a Krogh cylinder model in which vessels (red) run along the center axis of a tissue cylinder (gray). B) Depiction of a single vessel (red) supplying a cylindrical region of tissue (gray) with oxygen, where r is the radial coordinate, x is the distance along the network, r_t is the radius of the tissue region, r_v is the radius of the vessel, d is the tissue width and L is the vessel length. C) Distribution of the partial pressure of oxygen $PO_2(x,r)$ in the tissue surrounding the small arterioles in the radial direction at two fixed positions $x_{in,SA} = 0.81$ cm and $x_{end,SA} = 1.39$ cm, $PO_2(x_{in,SA}, r_v) = 67.53$ mmHg, $PO_2(x_{end,SA}, r_v) = 67.67$ mmHg, $M_0 = 1.65$ cm³ $O_2 \cdot 100$ cm⁻³ min⁻¹, $r_v = 23.6$ µm , $r_t = 38.6$ µm, $k = 9.4$ cm³ O_2 cm⁻¹ mmHg⁻¹ s⁻¹.

i, c_0 is the oxygen carrying capacity of red blood cells at 100% saturation, H_D is the discharge hematocrit, $S(x)$ is the blood oxygen saturation and q is the tissue oxygen consumption per vessel length. Since the clinical data set in this study does not include patient-specific hematocrit values, H_D is assumed to be constant, as specified in Table 3.

Oxygen consumption in the tissue is calculated using a Krogh cylinder model, in which each oxygen-delivering vessel is assumed to provide oxygen via diffusion to a cylindrical region of tissue surrounding it (see Fig. 2A). In the present model, oxygen is assumed to be delivered by the large and small arterioles and capillaries; no oxygen exchange is assumed in the venules. At each position x in the retinal vascular network, the oxygen is delivered to the nearest tissue via diffusion according to:

$$k\left[\frac{1}{r}\frac{d}{dr}\left(r\frac{dPO_2(x,r)}{dr}\right)\right] = M_0 \tag{2}$$

where k is the diffusion coefficient, PO_2 is the partial pressure of oxygen at a radial distance r within the tissue cylinder and M_0 is the tissue oxygen demand per tissue volume (assumed here to be constant). The degeneration of the retinal ganglion cells is modeled indirectly by varying the tissue oxygen demand M_0; retinal ganglion cells degeneration would correspond to a decrease in M_0. Given the architecture of this model, it is important to note that the M_0 defined here is primarily representative of the oxygen demand of the retinal ganglion cells in the inner retina.[28]

The partial pressure of oxygen in the tissue along the radial direction r for a fixed position in the network x is given by:

$$PO_2(x,r) = PO_2(x,r_{v,i}) + \frac{M_0}{k}\left[\frac{r^2 - r_{v,i}^2}{4} + \frac{r_{t,i}^2}{2}\ln\left(\frac{r_{v,i}}{r}\right)\right] \tag{3}$$

where the subscript i indicates the vessel compartment, $r_{t,i}$ denotes the radius of the tissue region and $r_{v,i}$ denotes the vessel radius, as depicted in Fig. 2B. Fig. 2C depicts a sample solution for two positions $x_{in,SA} = 0.81$ cm (blue curve) and $x_{end,SA} = 1.39$ cm (black curve) in the small arterioles for $PO_2(x_{in,SA}, r_v) = 67.53$ mmHg, $PO_2(x_{end,SA}, r_v) = 66.67$ mmHg, $M_0 = 1.65$ cm³ $O_2 \cdot 100$ cm⁻³ min⁻¹, $k = 9.4$ cm³ O_2 cm⁻¹ mmHg⁻¹ s⁻¹, $r_v = 23.6$ μm, and $r_t = 38.6$ μm.

For a constant value of M_0, the tissue oxygen consumption per vessel length (q) is computed as:

$$q(x) = \int_{r_{v,i}}^{r_{t,i}} M_0\, 2\pi r\, dr = \pi M_0\left(r_{t,i}^2 - r_{v,i}^2\right) \tag{4}$$

The width of tissue surrounding each vessel is defined as $d_i = r_{t,i} - r_{v,i}$. Here, it is assumed that d_i is equal to the same value d for each oxygen-delivering vessel i = LA, SA, C and that $d_i = 0$ for the SV and LV compartments. Thus, the oxygen consumption rate q depends on both the tissue volume surrounding the vessel and on the level of functional activity of the retinal ganglion cells represented by the tissue oxygen

demand (M_0). In turn, changes in the oxygen consumption rate q will induce changes in the oxygen saturation within the vessel as dictated by the balance of mass in Equation (1).

Given the model inputs listed in Table 1 section (a), the steady-state values of the diameters D_i and of the vascular smooth muscle activations A_i in the LA and SA compartments are determined by integrating the system of ordinary differential equation in Table 1(b) until equilibrium is reached. It is important to note that the system also involves the quantities T_i, $T_{total,i}$ and $A_{total,i}$ which, as detailed in Table 1, are functions of the unknowns D_i and A_i. The use of a steady state model is justified since the variation in the clinical measurements of oxygen saturation due to the cardiac cycle is not large.[29]

2.3 Model reference state

A reference state is defined to represent conditions typical of a healthy retina. For example, the reference state values of IOP, MAP and arterial and venous oxygen saturation are set equal to the average values of these factors measured in all of the healthy individuals in this study (see Table 5). The reference state value of tissue width is chosen to be $d^{ref} = 15$ μm, which corresponds to an experimental measurement of retinal intercapillary space of 30 μm.[30] In the reference state, the proportion of the tissue occupied by capillary lumens is about 2.7%, which is in good agreement with the proportion of 2.5% measured in histological specimens.[31] Given the reference

Table 5. Clinical average values of intraocular pressure (IOP, in mmHg), mean arterial pressure (MAP, in mmHg), ocular perfusion pressure (OPP = $\frac{2}{3}$ MAP – IOP, in mmHg), retinal arterial oxygen saturation and retinal venous oxygen saturation measured in healthy individuals, advanced (visual field MD ≥ 10 dB) primary open-angle glaucoma (POAG, IOP > 21 mmHg) patients and advanced normal tension glaucoma (NTG, IOP ≤ 21 mmHg) patients [4]. Reference state parameter values are highlighted in bold.

		Healthy (n=85)	Advanced POAG (n=12)	Advanced NTG (n=8)
Clinical data	IOP [mmHg]	**15 ± 3**	15 ± 3	10 ± 3
	MAP [mmHg]	**102 ± 12**	99 ± 10	109 ± 11
	OPP [mmHg]	**53 ± 8**	51 ± 8	62 ± 6
	Arterial oxygen saturation [%]	**93 ± 4**	95 ± 2	94 ± 3
	Venous oxygen saturation [%]	**54 ± 6**	58 ± 5	58 ± 6
Reference values	M_0^{ref} [$cm^3 O_2 \cdot 100\ cm^{-3} min^{-1}$]	**1.65**		
	d^{ref} [μm]	**15**		

values of IOP, MAP, tissue width, and arterial oxygen saturation, the model is used to calculate the value of tissue oxygen demand (M_0^{ref} = 1.65 cm³ O$_2$·100 cm^{-3} min^{-1}) that will yield the reference venous oxygen saturation level of 54%, as measured in healthy patients. This calculated rate of oxygen demand in the reference state is close in magnitude to oxygen demand levels observed experimentally.[32-34]

2.4 Model simulations

The mathematical model presented in this study is used to conduct the following simulations:

1. *Theoretical investigation*
    The model is used to predict the theoretical effect of the artificial variation of the model inputs (Table 1(a)) on the computed outputs (Table 1(g)).
2. *Theoretical interpretation of clinical data*
    The model is used to estimate patient-specific values of oxygen demand (simulation 2A) or tissue depth (simulation 2B) that would yield the clinically-measured value of venous oxygen saturation when patient-specific inputs are considered.

The details of the algorithms implemented to perform these novel, patient-specific simulations are provided below.

Algorithm for simulation 2A:
For any individual included in the experimental study proceed as follows:
  i.   Set the patient-specific input values for $P_{in,LA}$, $P_{out,LV}$ and $S(x=0)$ (Table 1(a)) given the clinical measurements of MAP, IOP and arterial oxygen saturation;
  ii. set the input tissue depth equal to the reference state value d^{ref} (Table 1(a));
  iii. set the initial guess for the input oxygen demand to M_0^0 (Table 1(a)), then for $k \geq 0$
    a. solve the model described in Table 1(b)-(f);
    b. compute the output of the model (Table 1(g)), which includes oxygen saturation $S^k(x)$;
    c. test for convergence:

    if $\dfrac{|\text{measured} - \text{predicted venous oxygen saturation}|}{|\text{measured venous oxygen saturation}|} \leq 5 \cdot 10^{-2}$, set $M_0 = M_k^0$,

    otherwise set $M_0^{(k+1)} = M_0^k + \delta_M$ and return to point a).

Algorithm for simulation 2B:
For any individual included in the experimental study proceed as follow:

i.   set the patient-specific input values for $P_{in,LA}$, $P_{out,LV}$ and $S(x=0)$ (Table 1(a)) given the clinical measurements of MAP, IOP and arterial oxygen saturation;
ii.   set the input oxygen demand equal to the reference state value M_0^{ref} (Table 1(a));
iii. set the initial guess for the input tissue depth to d^0 (Table 1(a)), then for $k \geq 0$
   a.   solve the model described in sections Table 1(b)-(f);
   b.   compute the output of the model (Table 1(g)), which includes oxygen saturation $S^k(x)$;
   c.   test for convergence:

   if $\dfrac{|\text{measured} - \text{predicted venous oxygen saturation}|}{|\text{measured venous oxygen saturation}|} \leq 5 \cdot 10^{-2}$, set $d = d^k$,

   otherwise set $d^{k+1} = d^k + \delta_d$ and return to point a).

In step iii(c) of simulations (2A) and (2B), the values of δ_M and δ_d are determined via the MATLAB algorithm fsolve, which is a nonlinear least-squares algorithm. For each of the algorithms (2A) and (2B), two sets of simulations are performed corresponding to the cases of functional or impaired autoregulation.

3. Results

3.1 Experimental data
Fig. 3 shows the scatter plot of the venous saturation data collected from healthy individuals, advanced POAG patients and advanced NTG patients.[4] Four healthy individuals and one advanced NTG patient were excluded since no record of MAP measurement was reported. Data for mild glaucoma patients are not included in the figure since Olafsdottir and Vandewalle *et al.*[4] found no statistical difference in retinal oxygen arterial and venous saturation between healthy individuals and mild glaucoma patients. The black bars represent the average value of each group and the corresponding standard deviation. In both the advanced POAG and advanced NTG patient groups, the average value of venous oxygen saturation is higher than in healthy individuals, and the average value of arteriovenous difference is lower than in healthy individuals. No statistical difference was reported in retinal oxygen saturation when mild POAG and mild NTG patients were compared, nor when advanced POAG and advanced NTG patients were compared. The average values of IOP, MAP and oxygen saturation measured in healthy individuals, advanced POAG patients and advanced NTG patients are also reported in Table 5.

3.2 Theoretical investigation
Fig. 4 shows the scatter plot of the venous oxygen saturation data collected from healthy individuals as a function of ocular perfusion pressure ($OPP = \frac{2}{3} MAP\text{-}IOP$). The
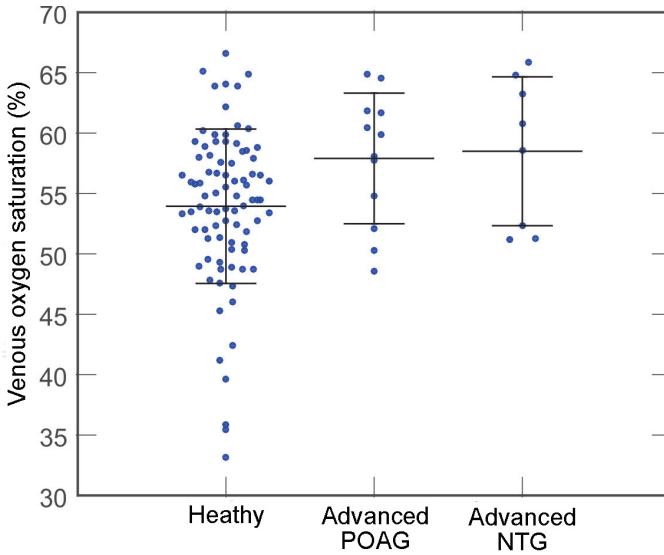
Fig. 3. Venous oxygen saturation clinical data collected from healthy individuals (n=85), advanced POAG patients (n=12) and advanced NTG patients (n=8)[4] (blue dots). Black bars represent the mean and standard deviation of each group.
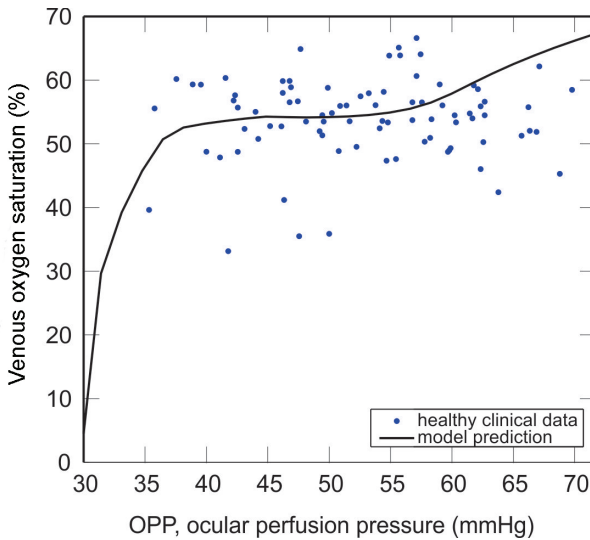
Fig. 4. A scatter plot of the venous saturation clinical data (blue dots) collected from healthy individuals is compared with theoretical predictions (solid black curve) as OPP is varied. Here, a range of OPP values is generated by holding IOP constant at its reference state value (15 mmHg) while varying MAP between 67 and 130 mmHg.

clinical data (blue dots) are compared to the mathematical model prediction (solid curve) of venous saturation as OPP is varied. Reference state values of IOP, MAP, arterial oxygen saturation, M_0^{ref} and d^{ref} are used to produce the model simulated curve. Since the model predictions generated by varying MAP and holding IOP constant or by varying IOP and holding MAP constant are nearly identical, only one curve is shown as OPP is varied.

Since the clinical data[4] show an increase in venous saturation in advanced glaucoma patients, the mathematical model is used to theorize three possible explanations for increased venous saturation:

1. **A decrease in tissue oxygen demand (M_0):** If less oxygen is consumed by the tissue, higher levels of venous oxygen saturation are predicted;
2. **An impairment of blood flow autoregulation:** If the most influential autoregulation mechanisms (conducted metabolic and/or local carbon dioxide response mechanisms) are impaired, higher levels of venous oxygen saturation are predicted for certain ranges of OPP;
3. **A decrease in tissue width (d):** If the volume of tissue supplied by each capillary or arteriole is decreased, higher levels of venous oxygen saturation are predicted.

As shown in Fig. 5A, the model predicts a decrease in venous oxygen saturation as oxygen demand is increased provided that all other factors (MAP, IOP, d, arterial blood saturation and functionality of autoregulation) are not altered. Fig. 5B depicts case (1) in which venous oxygen saturation is shown as a function of OPP for two different values of M_0: M_0^{ref} = 1.65 cm³ O₂·100 cm⁻³ min⁻¹(blue curve) and M_0 = 1.32 cm³ O₂·100 cm⁻³ min⁻¹ (red curve). These curves show the effect of a 20% decrease in oxygen demand on the model predictions of venous saturation. It is interesting to observe that this decrease in oxygen demand causes variable increases in venous oxygen saturation depending on the value of OPP.

Fig. 5C provides evidence for case (2), namely that an increase in venous oxygen saturation can also occur over a certain range of OPP values when autoregulation is impaired. In this case, M_0^{ref} = 1.65 cm³ O₂·100 cm⁻³ min⁻¹ for both curves, but the metabolic and carbon dioxide autoregulation mechanisms are impaired (*i.e.,* absent) in the black dashed curve.

Fig. 5D shows that a decrease in tissue width supplied by each arteriole or capillary in the Krogh cylinder model can also lead to an increase in venous oxygen saturation, as outlined in case (3). Decreasing the tissue width leads to a decrease in the total tissue volume supplied by the retinal vasculature. Fig. 5D depicts the effect of decreasing tissue width from d^{ref} = 15 *μm* (blue curve) to d = 13 *μm* (green curve).

3.3 Theoretical interpretation of clinical data

Fig. 6 summarizes the model predicted values of oxygen demand (gray) or tissue
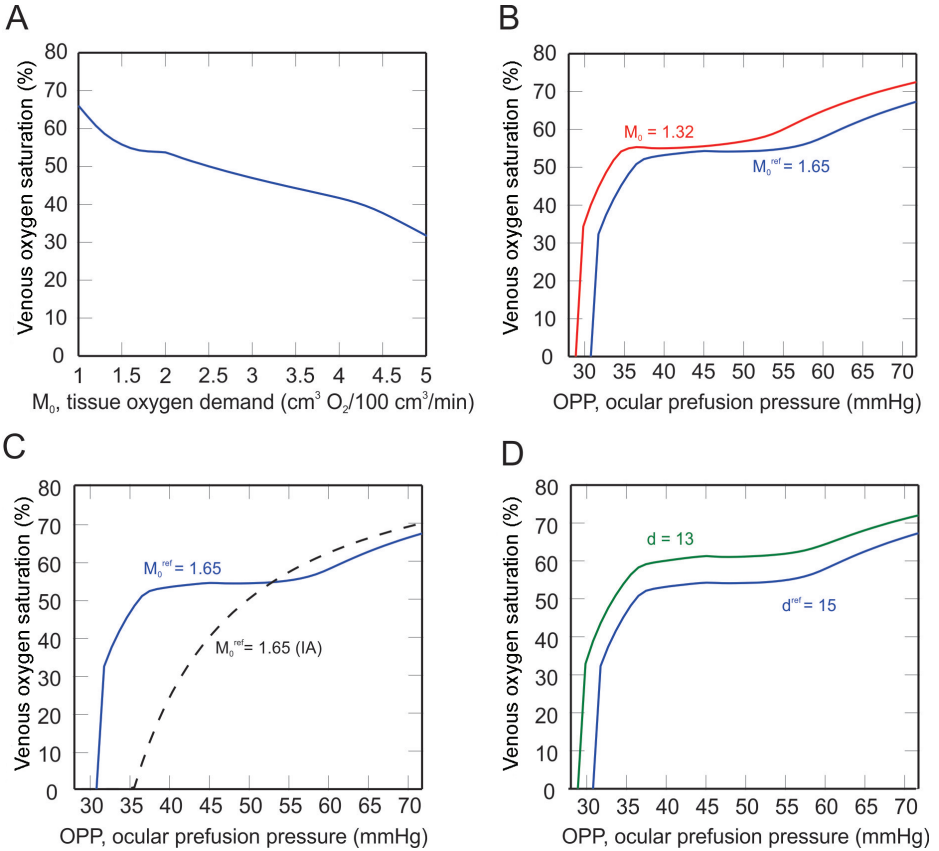
Fig. 5. A) Decrease in venous oxygen saturation as tissue oxygen demand (M_0) is increased, given constant reference state values of MAP, IOP and arterial oxygen saturation. The remaining panels highlight the three-part theoretical investigation of the effects of B) oxygen demand (M_0), C) impaired autoregulation (IA) and D) tissue width (d) on model predictions of venous oxygen saturation as OPP is varied. Each scenario is compared with the model prediction of the reference state (blue curve) in which M_0^{ref} = 1.65 cm³ O_2/100 cm³/min, d^{ref} = 15 μm, and autoregulation is functional.

width (blue) that will yield the clinically observed venous saturation levels (Fig. 3) for each individual in the healthy, advanced POAG and advanced NTG populations. Model predictions for mild POAG and NTG patient groups are not included since the venous saturation levels did not differ from healthy individuals. The model predicts that the observed increase in venous saturation in advanced POAG patients is accompanied by a decrease in oxygen demand, whereas no change in oxygen demand is predicted in advanced NTG patients. A slightly lower tissue width is predicted in POAG patients to yield increased venous saturation but not
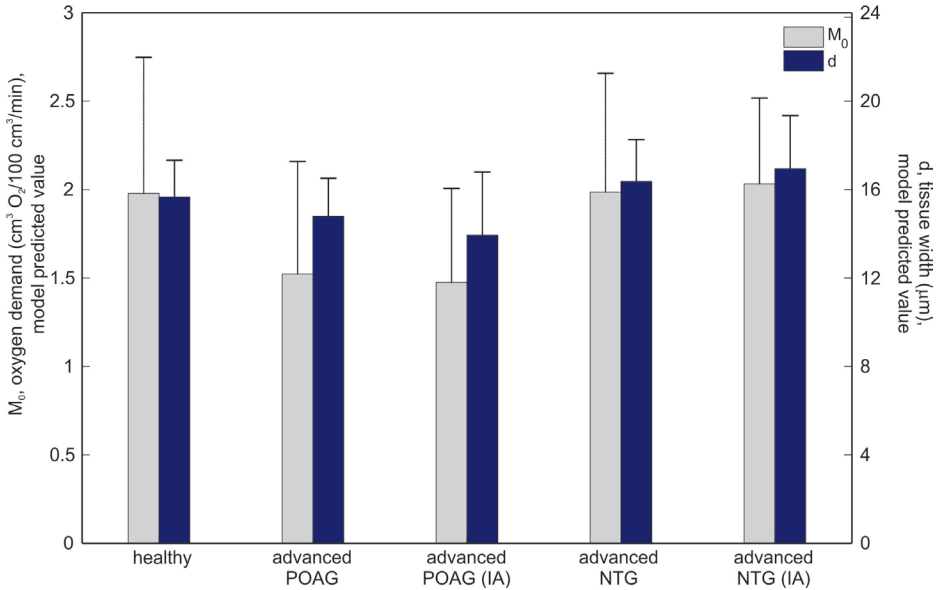
Fig. 6. Model predicted levels of tissue oxygen demand (M_0) and tissue width (d) that yield the venous saturation clinical data collected from each individual in the healthy, advanced POAG and advanced NTG populations.[4] Model predictions are also provided when autoregulation is impaired (IA) in advanced POAG and NTG patients. Black bars represent mean and standard deviation of each group.

in NTG patients. These trends are observed regardless of whether autoregulation is functioning or impaired. Table 6 lists the mean and standard deviation of the oxygen demand and tissue width model predictions depicted in Fig. 6. All clinical measures were used except for a few cases in which the tolerance of the optimization procedure employed to find M_0 (2 healthy patients, 1 advanced POAG patient and 1 advanced NTG patient) and d (2 healthy patients and 1 advanced NTG patient) was not achieved.

Table 6. Model predicted levels of tissue oxygen demand (M_0) and tissue width (d) that yield the venous saturation clinical data collected from healthy, advanced POAG and advanced NTG patients. [4]

	Healthy	Advanced POAG	Advanced POAG (IA)	Advanced NTG	Advanced NTG (IA)
M_0 [cm³ O₂·100 cm⁻³ min⁻¹]	1.98 ± 0.77	1.52 ± 0.64	1.48 ± 0.53	1.99 ± 0.67	2.03 ± 0.48
d [μm]	15.66 ± 1.66	14.79 ±1.72	13.94 ± 2.85	16.36 ±1.90	16.94 ±2.40

It is important to note that the average values of oxygen demand and tissue width calculated for the healthy population (reported in Table 6) are not equal to the reference state values of oxygen demand and tissue width (reported in Table 5). In Table 5, the values M_0^{ref} and d^{ref} are computed from average values of IOP, MAP and arterial saturation obtained from the healthy population. In Table 6, the values of M_0 and d are computed using the MAP, IOP and arterial saturation from each individual and then averaging the resulting values in each population.

Based on the model predictions summarized in Fig. 6 and Table 6, Fig. 7A shows the model predicted curves of venous oxygen saturation for $M_0 = 1.98$ cm³ $O_2 \cdot 100$ cm⁻³ min⁻¹ (blue curve) and decreased $M_0 = 1.52$ cm³ $O_2 \cdot 100$ cm⁻³ min⁻¹ (black curve) as well as the average clinical values of venous saturation and OPP in healthy individuals (asterisk) and advanced POAG patients (square). In Fig. 7B, $M_0 = 1.98$ cm³ $O_2 \cdot 100$ cm⁻³ min⁻¹ and $d^{ref} = 15$ μm are fixed for both curves, but autoregulation is assumed to be impaired for the black dashed curve. These model predictions are compared with average clinical values of venous saturation and OPP measured in healthy individuals (asterisk) and advanced NTG patients (square).
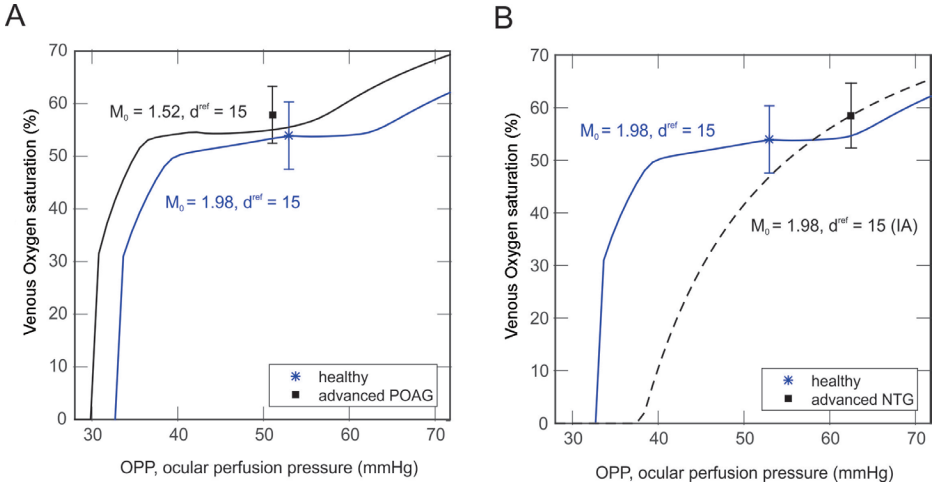
Fig. 7. Model predicted curves of venous oxygen saturation as OPP is varied are shown with average values of venous oxygen saturation and OPP measured clinically. A) The observed increase in the average venous saturation in healthy individuals (blue asterisk) and in advanced POAG patients (black square) is compared with model predicted levels of venous saturation for decreased levels of tissue demand. B) The observed increase in the average venous saturation in healthy individuals (blue asterisk) and advanced NTG patients (black square) is compared with model predicted levels of venous saturation when autoregulation is impaired (IA).

4. Discussion

4.1 Experimental data

Retinal vessel oxygen saturation was measured in healthy individuals and glaucoma patients using a non-invasive retinal oximeter. The measurements indicated that patients with advanced glaucoma (both POAG and NTG patients) exhibited higher venous oxygen saturation (and consequently a lower arteriovenous difference in oxygen saturation) compared with healthy individuals. Other studies[21,22] have confirmed these findings, and it has been previously hypothesized[4] that the observed increase in venous saturation is likely a secondary effect of glaucomatous atrophy and not a primary cause of glaucoma, citing the absence of hypoxia in advanced glaucoma patients as supporting evidence. However, the number of advanced glaucoma patients in these studies (including the current one) was rather small, and many patients were under active ophthalmological care. Thus, additional studies, ideally progressive in nature and conducted in patients with very high IOP and very low OPP, are needed in order to draw more definitive conclusions.

4.2 Theoretical investigation

This study implements a theoretical model based on fundamental hemodynamic and mechanical principles to predict venous oxygen saturation levels given patient-specific values of MAP, IOP and arterial oxygen saturation. The model predictions using the reference state values of these factors align well with the observed venous saturation levels collected from healthy individuals (Fig. 4).

A Krogh cylinder model is used to describe the diffusion of oxygen into tissue; this Krogh model is applied in the classical sense in which the oxygen-supplying vessel runs along the central axis of a tissue cylinder. However, such an assumption may not be the most appropriate for retinal tissue, since the majority of the tissue that retinal vessels feed is typically located "below" the vessels.[35] Some mathematical models have described oxygen diffusion through the retinal tissue layers[36-39] but did not consistently include a description of blood flow and autoregulation in the retinal vasculature. It would be an interesting research direction to enhance the model in the current study to include a more realistic geometric arrangement of vessels and tissue. It has also been shown that oxygen diffuses directly from the CRA to the CRV, bypassing the retinal microcirculation, due to the close anatomical relation between the central retinal vessels in the center of the optic nerve.[40,41] The current model could be extended to include the effects of this counter-current exchange phenomenon.

4.3 Theoretical interpretation of clinical data

In this study, a mathematical model is used to offer possible explanations for the observed trends in oximetry data collected in healthy individuals and glaucoma patients. Specifically, the model shows that a decrease in oxygen demand, an

impairment of autoregulation or a decrease in tissue width can all lead to increased venous saturation levels. It is important to note that although the model predictions offer each of these scenarios as a possible explanation, not all of them are physiologically relevant when describing the details of glaucoma. For example, suggesting a decrease in the Krogh cylinder tissue width as an explanation for the increased venous saturation levels observed in glaucoma is not consistent with the reduced vascularization observed in some glaucoma patients.[14-16,31] However, the interconnection of tissue width and retinal atrophy suggests that future insight could be gained by using the model to assess the effects of altering multiple factors at once.

The patient-specific model optimizations presented in this study (Fig. 7) suggest that there might be different explanations for the increased venous saturation levels observed among advanced POAG patients and advanced NTG patients. Specifically, a decrease in oxygen demand may be more relevant to the increase in venous saturation observed in advanced POAG (Fig. 7A), while impaired autoregulation mechanisms may be more relevant to the increase in venous saturation observed in advanced NTG (Fig. 7B). This finding also suggests that vascular changes might occur primary to glaucomatous damage in NTG patients. Of note, the relation found between NTG patients and the impairment of blood flow autoregulation has been proposed previously.[42,43] Importantly, impaired blood flow autoregulation could play a role in all advanced glaucoma patients, but to varying extents, as suggested by Fig. 6. Additional theoretical investigations, ideally coupled with statistical methods and conducted on a wider set of glaucoma patients, are needed to confirm the model findings.

In a study that measured venous oxygen saturation under altered light and dark conditions,[44] an increase in arterial and venous saturation was observed, although the arteriovenous difference in oxygen saturation was reported to be stable. The authors hypothesized that the observed increase in venous saturation was accompanied by an increase in oxygen consumption, which opposes the hypothesis offered in the current study. However, in the light and dark study,[44] the oxygen demand increased mostly in the outer retina due to the increased photoreceptor activity. The outer retina is not directly accounted for in the model presented here, which therefore may limit the possible model predictions under various conditions. Additionally, it is possible that a compromised ocular circulation renders an individual more susceptible to a given IOP, thereby representing a confounding factor that falls outside of strict primary or secondary classifications.

5. Conclusions

Overall, this model provides an important step in assessing and quantifying observations in clinical data. Instead of performing statistical analyses on measured observations, the model provides a mechanical framework built upon blood flow

principles that can be used to make independent predictions of the same measured quantities while varying MAP, IOP and arterial oxygen saturation. Overall, the study suggests that the primary mechanisms leading to increased venous saturation in advanced cases of glaucoma might differ between POAG and NTG patients. It is hypothesized that the increased saturation levels are more likely to be explained by decreased oxygen demand in POAG patients and impaired autoregulation in NTG patients. In future studies, the model will continue to be used to address the open question of whether vascular changes occur primary or secondary to glaucomatous damage, possibly identifying subgroups of patients where vascular pathogenic mechanisms play a more significant role. However, progressive data and larger data sets are needed to confirm the hypotheses formulated on the basis of the model predictions.

Acknowledgments

References

1. Moore D, Harris A, Wudunn D, Kheradiya N, Siesky B. Dysfunctional regulation of ocular blood flow: A risk factor for glaucoma? Clin Ophthalmol 2008;2(4):849-861. Available from: http://www.dovepress.com/articles.php?article_id=411 PubMed PMID: 19668439.
2. Harris A, Kagemann L, Ehrlich R, Rospigliosi C, Moore D, Siesky B. Measuring and interpreting ocular blood flow and metabolism in glaucoma. Can J Ophthalmol 2008;43(3):328-336. Available from: http://linkinghub.elsevier.com/retrieve/pii/S0008418208801147 PubMed PMID: 18443609. doi: 10.3129/i08-051.
3. Olafsdottir OB, Hardarson SH, Gottfredsdottir MS, Harris A, Stefansson E. Retinal oximetry in primary open-angle glaucoma. Invest Ophthalmol Vis Sci 2011;52(9):6409-13. Available from: http://iovs.arvojournals.org/article.aspx?doi=10.1167/iovs.10-6985 doi: 10.1167/iovs.10-6985.
4. Olafsdottir OB, Vandewalle E, Abegao Pinto L, et al. Retinal oxygen metabolism in healthy subjects and glaucoma patients. Br J Ophthalmol 2014;98(3):329-333. Available from: http://bjo.bmj.com/cgi/doi/10.1136/bjophthalmol-2013-303162 PubMed PMID: 24403567. doi: 10.1136/bjophthalmol-2013-303162.

5. Geirsdottir A, Hardarson SH, Olafsdottir OB, Stefansson E. Retinal oxygen metabolism in exudative age-related macular degeneration. Acta Ophthalmol 2014;92(1):27-33. Available from: http://dx.doi.org/10.1111/aos.12294 PubMed PMID: 24447786. doi: 10.1111/aos.12294.

6. Michelson G, Scibor M. Intravascular oxygen saturation in retinal vessels in normal subjects and open-angle glaucoma subjects. Acta Ophthalmol Scand 2006 Apr;84(3):289-295. Available from: http://doi.wiley.com/10.1111/j.1600-0420.2005.00631.x PubMed PMID: 16704685. doi: 10.1111/j.1600-0420.2005.00631.x.

7. Abegao Pinto L, Vandewalle E, De Clerck E, Marques-Neves C, Stalmans I. Ophthalmic artery Doppler waveform changes associated with increased damage in glaucoma patients. Invest Ophthalmol Vis Sci 2012 Apr;53(4):2448-53. Available from: http://www.diseaseinfosearch.org/result/3065 PubMed PMID: 22427555. doi: 10.1167/iovs.11-9388.

8. Akarsu C, Bilgili MY. Color Doppler imaging in ocular hypertension and open-angle glaucoma. Graefes Arch Clin Exp Ophthalmol 2004;242(2):125-9. Available from: http://link.springer.com/10.1007/s00417-003-0809-3 PubMed PMID: 7940146. doi: 10.1007/s00417-003-0809-3.

9. Butt Z, O'Brien C, McKillop G, Aspinall P, Allan P. Color Doppler imaging in untreated high- and normal-pressure open-angle glaucoma. Invest Ophthalmol Vis Sci 1997;38(3):690-6. Available from: http://www.diseaseinfosearch.org/result/3065 PubMed PMID: 9071223. doi: 10.1364/BOE.3.003127.

10. Rojanapongpun P, Drance SM, Morrison BJ. Ophthalmic artery flow velocity in glaucomatous and normal subjects. Br J Ophthalmol 1993;77(1):25-29. Available from: http://bjo.bmj.com/cgi/doi/10.1136/bjo.77.1.25 PubMed PMID: 8435394. doi: 10.1136/bjo.77.1.25.

11. Tobe LA, Harris A, Hussain RM, et al. The role of retrobulbar and retinal circulation on optic nerve head and retinal nerve fibre layer structure in patients with open-angle glaucoma over an 18-month period. Br J Ophthalmol 2015;99(5):609-612. Available from: http://bjo.bmj.com/cgi/doi/10.1136/bjophthalmol-2014-305780 PubMed PMID: 25467967. doi: 10.1136/bjophthalmol-2014-305780.

12. Grieshaber MC, Flammer J. Blood flow in glaucoma. Curr Opin Ophthalmol 2005;16(2):79-83. Available from: http://content.wkhealth.com/linkback/openurl?sid=WKPTLP:landingpage&an=00055735-200504000-00002 PubMed PMID: 15744136. doi: 10.1097/01.icu.0000156134.38495.0b.

13. Flammer J. The vascular concept of glaucoma. Surv Ophthalmol 1994;38 Suppl(38):105-10.

14. Jia Y, Morrison JC, Tokayer J, Tan O, Lombardi L, Baumann B, et al. Quantitative OCT angiography of optic nerve head blood flow. Biomed Opt Express 2012;3(12):3127-37. Available from: http://europepmc.org/abstract/MED/23243564 PubMed PMID: 23243564. doi: 10.1364/BOE.3.003127.

15. Jia Y, Tan O, Tokayer J, et al. Split-spectrum amplitude-decorrelation angiography with optical coherence tomography. Opt Express 2012;20(4):4710-25. Available from: http://europepmc.org/abstract/MED/22418228 PubMed PMID: 22418228. doi: 10.1364/OE.20.004710.

16. Jia Y, Wei E, Wang X, et al. Optical coherence tomography angiography of optic disc perfusion in glaucoma. Ophthalmol 2014;121(7):1322-1332. Available from: http://europepmc.org/abstract/MED/24629312 PubMed PMID: 24629312. doi: 10.1016/j.ophtha.2014.01.021.

17. Harris A, Jonescu-Cuypers C, Kagemann L, Ciulla T, Krieglstein G. International ophthalmology. Atlas of ocular blood flow: Butterworth-Heinemann; 2003. Available from: http://antibodies.cancer.gov/apps/site/detail/CPTC-GSTMu1-6 PubMed PMID: 11944858. doi: 10.1023/A:1014402730503 .

18. Weinreb R, Harris A. Ocular blood flow in glaucoma: The 6th consensus report of the world glaucoma association. Amsterdam, The Netherlands: Kugler Publications; 2009.

19. Ito M, Murayama K, Deguchi T, et al. Oxygen saturation levels in the juxta-papillary retina in eyes with glaucoma. Exp Eye Res 2008;86(3):512-518. Available from: http://linkinghub.elsevier.com/retrieve/pii/S0014483507003715 PubMed PMID: 18262523. doi: 10.1016/j.exer.2007.12.010.

20. Vandewalle E, Abegao Pinto L, et al. Oximetry in glaucoma: correlation of metabolic change with structural and functional damage. Acta Ophthalmol 2014;92(2):105-110. Available from: http://dx.doi.org/10.1111/aos.12011 PubMed PMID: 23323611. doi: 10.1111/aos.12011.

21. Mordant DJ, Al-Abboud I, Muyo G, Gorman A, Harvey AR, McNaught AI. Oxygen saturation measure-

ments of the retinal vasculature in treated asymmetrical primary open-angle glaucoma using hyperspectral imaging. Eye 2014 Jul;28(10):1190-1200. Available from: http://europepmc.org/abstract/MED/25060843 PubMed PMID: 25060843. doi: 10.1038/eye.2014.169.

22. Ramm L, Jentsch S, Peters S, Augsten R, Hammer M. Investigation of blood flow regulation and oxygen saturation of the retinal vessels in primary open-angle glaucoma. Graefes Arch Clin Exp Ophthalmol 2014;252(11):1803-1810. Available from: http://www.diseaseinfosearch.org/result/3065 PubMed PMID: 25112846. doi: 10.1007/s00417-014-2766-4.

23. Arciero J, Harris A, Siesky B, Amireskandari A, Gershuny V, Pickrell A, et al. Theoretical analysis of vascular regulatory mechanisms contributing to retinal blood flow autoregulation. Invest Ophthalmol Vis Sci 2013 Aug;54(8):5584-93. Available from: http://europepmc.org/abstract/MED/23847315 PubMed PMID: 23847315. doi: 10.1167/iovs.12-11543.

24. Pries AR, Secomb TW, Gessner T, Sperandio MB, Gross JF, Gaehtgens P. Resistance to Blood-Flow in Microvessels in-Vivo. Circ Res 1994;75(5):904-915. Available from: http://circres.ahajournals.org/cgi/pmidlookup?view=long&pmid=7923637 PubMed PMID: 7923637. doi: 10.1161/01.RES.75.5.904.

25. Ye GF, Moore TW, Buerk DG, Jaron D. A compartmental model for oxygen-carbon dioxide coupled transport in the microcirculation. Ann Biomed Eng 1994;22(5):464-479. Available from: http://link.springer.com/10.1007/BF02367083 PubMed PMID: 7825749. doi: 10.1007/BF02367083.

26. Orgul S, Cioffi GA, Wilson DJ, Bacon DR, Van Buskirk EM. An endothelin-1 induced model of optic nerve ischemia in the rabbit. Invest Ophthalmol Vis Sci 1996;37(9):1860-9.

27. Orgul S, Gugleta K, Flammer J. Physiology of perfusion as it relates to the optic nerve head. Surv Ophthalmol 1999;43 Suppl 1(43):592-8. Available from: http://toxnet.nlm.nih.gov/cgi-bin/sis/search2/r?dbs+hsdb:@term+@rn+7782-44-7 PubMed PMID: 10416744.

28. Causin P, Guidoboni G, Malgaroli F, Sacco R, Harris A. Blood flow mechanics and oxygen transport and delivery in the retinal microcirculation: multiscale mathematical modeling and numerical simulation. Biomech Model Mechanobiol 2015 Aug;36:247-259. Available from: http://linkinghub.elsevier.com/retrieve/pii/S135094621300044X PubMed PMID: 26232093. doi: 10.1007/s10237-015-0708-7.

29. Palsson O, Geirsdottir A, Hardarson SH, Olafsdottir OB, Kristjansdottir JV, Stefansson E. Retinal oximetry images must be standardized: a methodological analysis. Invest Ophthalmol Vis Sci 2012 Apr;53(4):1729-33. Available from: http://toxnet.nlm.nih.gov/cgi-bin/sis/search2/r?dbs+hsdb:@term+@rn+7782-44-7 PubMed PMID: 22395877. doi: 10.1167/iovs.11-8621.

30. Michelson G, Welzenbach J, Pal I, Harazny J. Functional imaging of the retinal microvasculature by scanning laser Doppler flowmetry. Int J Ophthalmol 2001;23(4-6):327-335. Available from: http://antibodies.cancer.gov/apps/site/detail/CPTC-GSTMu1-6 PubMed PMID: 11944858. doi: 10.1023/A:1014402730503.

31. Quigley HA. Neuronal death in glaucoma. Prog Retin Eye Res 1999;18(3):39-57. Available from: http://linkinghub.elsevier.com/retrieve/pii/S0014483505801228 PubMed PMID: 9920498. doi: 10.1016/S0014-4835(05)80122-8.

32. Medrano CJ, Fox DA. Oxygen consumption in the rat outer and inner retina: light- and pharmacologically-induced inhibition. Exp Eye Res 1995;61(3):273-284. Available from: http://linkinghub.elsevier.com/retrieve/pii/S0014483505801228 PubMed PMID: 7556491. doi: 10.1016/S0014-4835(05)80122-8.

33. Braun RD, Linsenmeier RA, Goldstick TK. Oxygen consumption in the inner and outer retina of the cat. Invest Ophthalmol Vis Sci 1995;36(3):542-54. Available from: http://www.scholaruniverse.com/ncbi-linkout?id=12695252 PubMed PMID: 12695252. doi: 10.1001/archopht.121.4.547.

34. Wangsa-Wirawan ND, Linsenmeier RA. Retinal oxygen: fundamental and clinical aspects. Arch Ophthalmol 2003;121(4):547-57. Available from: http://www.scholaruniverse.com/ncbi-linkout?id=12695252 PubMed PMID: 12695252. doi: 10.1001/archopht.121.4.547.

35. Kur J, Newman EA, Chan-Ling T. Cellular and physiological mechanisms underlying blood flow regulation in the retina and choroid in health and disease. Prog Retin Eye Res 2012;31(5):377-406. Available from: http://linkinghub.elsevier.com/retrieve/pii/S1350946212000298 PubMed PMID: 22580107. doi: 10.1016/j.preteyeres.2012.04.004.

36. Cringle SJ, Yu DY. A multi-layer model of retinal oxygen supply and consumption helps explain the muted rise in inner retinal PO(2) during systemic hyperoxia. Comp Biochem Physiol A Mol Integr Physiol 2002;132(1):61-66. Available from: http://linkinghub.elsevier.com/retrieve/pii/S109564330100530X PubMed PMID: 12062192. doi: 10.1016/S1095-6433(01)00530-X.

37. Haugh LM, Linsenmeier RA, Goldstick TK. Mathematical models of the spatial distribution of retinal oxygen tension and consumption, including changes upon illumination. Ann Biomed Eng 1990;18(1):19-36. Available from: http://www.scholaruniverse.com/ncbi-linkout?id=2306030 PubMed PMID: 2306030. doi: 10.1007/BF02368415.

38. Lau JC, Linsenmeier RA. Oxygen consumption and distribution in the Long-Evans rat retina. Exp Eye Res 2012;102(5):50-58. Available from: http://linkinghub.elsevier.com/retrieve/pii/S001448351200190X PubMed PMID: 22828049. doi: 10.1016/j.exer.2012.07.004.

39. Roos MW. Theoretical estimation of retinal oxygenation during retinal artery occlusion. Physiol Measol 2004;25(6):1523-1532. Available from: http://toxnet.nlm.nih.gov/cgi-bin/sis/search2/r?dbs+hsdb:@term+@rn+7782-44-7 PubMed PMID: 15712729. doi: 10.1088/0967-3334/25/6/016.

40. Riva CE, Pournaras CJ, Tsacopoulos M. Regulation of local oxygen tension and blood flow in the inner retina during hyperoxia. J Appl Physiol 1986;61(2):592-8. Available from: http://toxnet.nlm.nih.gov/cgi-bin/sis/search2/r?dbs+hsdb:@term+@rn+7782-44-7 PubMed PMID: 3745049.

41. Bek T. Regional morphology and pathophysiology of retinal vascular disease. Prog Retin Eye Res 2013;36:247-259. Available from: http://linkinghub.elsevier.com/retrieve/pii/S135094621300044X PubMed PMID: 23892140. doi: 10.1016/j.preteyeres.2013.07.002.

42. Abegao Pinto L, Vandewalle E, De Clerck E, Marques-Neves C, Stalmans I. Lack of spontaneous venous pulsation: possible risk indicator in normal tension glaucoma. Acta Ophthalmol 2013;91(6):514-520. Available from: http://dx.doi.org/10.1111/j.1755-3768.2012.02472.x PubMed PMID: 22776135. doi: 10.1111/j.1755-3768.2012.02472.x.

43. Oettli A, Gugleta K, Kochkorov A, Katamay R, Flammer J, Orgul S. Rigidity of retinal vessel in untreated eyes of normal tension primary open-angle glaucoma patients. J glaucoma 2011;20(5):303-306. Available from: http://content.wkhealth.com/linkback/openurl?sid=WKPTLP:landing-page&an=00061198-201106000-00007 PubMed PMID: 20577102. doi:10.1097/IJG.0b013e3181e666a1.

44. Hardarson SH, Basit S, Jonsdottir TE, et al. Oxygen saturation in human retinal vessels is higher in dark than in light. Invest Ophthalmol Vis Sci 2009;50(5):2308-11. Available from: http://iovs.arvojournals.org/article.aspx?doi=10.1167/iovs.08-2576 doi: 10.1167/iovs.08-2576.